ACS APPLIED MATERIALS & INTERFACES

Research Article

www.acsami.org

Fluorescent Hydrogels with Tunable Nanostructure and Viscoelasticity for Formaldehyde Removal

Shasha Song, Aixin Song, Lei Feng, Guangcheng Wei, Shuli Dong, and Jingcheng Hao*

Key Laboratory of Colloid and Interface Chemistry & Key Laboratory of Special Aggregated Materials, Shandong University, Ministry of Education, Jinan 250100, China

Supporting Information

ABSTRACT: Hydrogels with ultrahigh water content, ~99 wt %, and highly excellent mechanical strength were prepared by 4′-*para*-phenylcarboxyl-2,2′:6′,2″-terpyridine (PPCT) in KOH aqueous solution. The self-assembled structure, rheological properties, and the gel−sol transformation temperature ($T_{gel-sol}$) of PPCT/KOH hydrogels that depend on PPCT and KOH concentrations were studied, indicating easily controllable conditions for producing hydrogels in PPCT and KOH mixtures. An important finding was that the hydration radius (R_h) of cations (M^+ = Li^+, Na^+, K^+, Cs^+, NH_4^+, $(CH_3)_4N^+$, $(CH_3CH_2)_4N^+$, $(CH_3CH_2CH_2)_4N^+$, $(CH_3CH_2CH_2CH_2)_4N^+$) plays a vital role in gelation of PPCT/MOH systems. To produce hydrogels in PPCT/MOH systems, the R_h of M^+ must be in a suitable region of 3.29 to 3.58 Å, e.g., K^+, Na^+, Cs^+, and the capability of M^+ for inducing PPCT to form hydrogels is K^+ > Na^+ > Li^+, which is followed by the Hofmeister series. The hydrogels of PPCT and KOH mixtures are responsive to external stimuli including temperature and shearing force, and present gelation-induced enhanced fluorescence emission property. The states of being sensitive to the stimuli can readily recover to the original hydrogels, which are envisaged to be an attracting candidate to produce self-healing materials. A typical function of the hydrogels of PPCT and KOH mixtures is that formaldehyde (HCHO) can speedily be adsorbed via electrostatic interaction and converted into nontoxic salts (HCOOK and CH_3OK), making it a promising candidate material for HCHO removal in home furnishings to reduce indoor environmental pollutants.

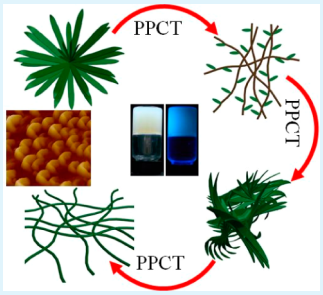

KEYWORDS: *viscoelastic hydrogels, Hofmeister series, molecular self-assembly, mechanical strength, stimuli-responsive, HCHO removal*

1. INTRODUCTION

The concept of self-assembly is that small structural units, e.g., atoms, molecules, macroions or nanoclusters, self-organize into more complicated structrues through nonconvalent interactions.[1] As one of the most urgent concerns in the sciences of the 21st century, molecular self-assembly has been considered as an attractive, practical, bottom-up approach to obtain stable, structurally well-defined, and functional objects at the nano- and microscale in biological systems and materials synthesis.[1−3] For self-assembled nanostructure materials, one of the challenges is how to design the component systems to acquire the desired patterns and functions.[4] As the important materials, hydrogels originating from amphiphilic systems have been attracted much attention since they are essentially green soft materials composed of a large amounts of water (>90 wt %) and small part of organic species.[5] Because of the high water content, hydrogels can be utilized to emulate the physical properties of soft tissues, e.g., cartilage, muscle, and eyeball, making them highly suitable as scaffolds for tissues engineering, and can apply to diapers, contact lenses, drug reservoirs, etc.[6] Moreover, the well-ordered structures of hydrogels play crucial role in executing the functions of living organisms. Generally, hydrogels are always composed of three-dimensional (3D) cross-linked networks formed by interweaving of fibers or nanotubes, which restrict their applications in tissues engineering and nanosciences.[5,7,8] The design of amphiphiles with special functional groups for constructing hydrogels with fascinating and novel structures is required to achieve functional applications.

Recently, fluorescent self-assembled hydrogels constructed from π-conjugated gelators have received particular attention due to their special luminescence property and promising applications in optoelectronics and fluorescence sensors.[9] Most π-conjugated molecules undergo a emission quenching in solution state, while formed hydrogels, the molecules exhibit enhanced emission due to the π−π stacking, which is referred as "gelation-enhanced emission".[10] The metal−ligand combination has been considered as an excellent π-conjugated gelator to fabricate fluorescent hydrogels owing to its easy regulation in gelation. Terpyridine (TP), a typical π-conjugated molecule, has rich coordination and high binding affinity with metal ions, making it become an excellent gelator to produce fluorescent hydrogels.

Herein, we synthesized the terpyridine (TP) derivative, 4′-*para*-phenylcarboxyl-2,2′:6′,2″-terpyridine (PPCT), and investigated the gelation behavior of the mixtures of PPCT and

Received: August 23, 2014
Accepted: October 3, 2014
Published: October 3, 2014

   dx.doi.org/10.1021/am505701u | ACS Appl. Mater. Interfaces 2014, 6, 18319−18328

MOH (M^+ = Li^+, Na^+, K^+, Cs^+, NH_4^+, $(CH_3)_4N^+$, $(CH_3CH_2)_4N^+$, $(CH_3CH_2CH_2)_4N^+$, $(CH_3CH_2CH_2CH_2)_4N^+$) in aqueous solutions. An important finding was that the hydration radius (R_h) of monovalent cations plays a vital role in gelation of PPCT/MOH systems. The capability of M^+ for inducing PPCT to form hydrogels is $K^+ > Na^+ > Li^+$, which is followed by the Hofmeister series. Due to the ultragelation capability of the PPCT/KOH system, the hydrogels with ultrahigh water content, ~99 wt %, and high mechanical strength can be facilely prepared by adding PPCT in KOH aqueous solution. The hydrogels of PPCT and KOH mixtures containing nanoflowers which are viscoelastic and have the yield stress to be 7000 Pa are responsive to external stimuli including temperature and shearing force and can readily recover to its original states. A typical function of the hydrogels is that formaldehyde (HCHO) can speedily be adsorbed via electrostatic interaction and converted into nontoxic salts (HCOOK and CH_3OK), making it a promising candidate material for HCHO removal in home furnishings to reduce indoor environmental pollutants.

2. EXPERIMENTAL SECTION

Chemicals and Materials. 4′-*para*-Phenylcarboxyl-2,2′:6′,2″-terpyridine (PPCT) was synthesized according to the literature.[11,12] Lithium hydroxide (LiOH, >99%), sodium hydroxide (NaOH, >98%), potassium hydroxide (KOH, >96%), and cesium hydroxide (CsOH, >99%) were purchased from Aladdin (Shanghai, China). Tetramethylammonium hydroxide (Me_4NOH, 25 wt %), tetraethylammonium hydroxide (Et_4NOH, 25 wt %), tetrapropylammonium hydroxide (Pr_4NOH, 25 wt %), and tetrabutylammonium hydroxide (Bu_4NOH, 25 wt %), and acetylacetone (>99%) were purchased from J&K Chemical Company, Ltd. (China). Potassium dichromate, potassium iodide, sodium thiosulfate, and ammonium acetate were purchased from Sinopharm Chemical Reagent Co., Ltd. (Shanghai, China) and were of pro analysis quality. Ultrapure water with a resistivity of 18.25 mΩ·cm was obtained using a UPH-IV ultrapure water purifier (Chengdu Ultrapure Technology Co. Ltd., China).

Sample Preparation. The samples were prepared by mixing appropriate amounts of PPCT and MOH (M^+ = Li^+, Na^+, K^+, Cs^+, NH_4^+, $(CH_3)_4N^+$, $(CH_3CH_2)_4N^+$, $(CH_3CH_2CH_2)_4N^+$, $(CH_3CH_2CH_2CH_2)_4N^+$) in water, and followed by stirring at room temperature until PPCT was dissolved completely. All the samples were equilibrated at T = 25.0 ± 0.1 °C for at least 2 weeks before the gelation behavior was inspected.

Transmission Electron Microscopy (TEM). For TEM observation, a small volume of gel sample was placed on TEM grids (copper grid, 3.02 mm, 200 meshes, coated with formvar film) and the excess solution was wiped away with a filter paper. The copper grids were frozen in a vacuum extractor at −55 °C for 3 days. Then the copper grids were observed on a JEOL JEM-1400 TEM operating at 120 kV. The images were recorded on a Gatan multiscan CCD and processed with a digital micrograph.

Field-Emission Scanning Electron Microscopy (FE-SEM). A small volume of gel sample was placed on a silica wafer, and most of the colloid gel was removed using small forceps to form a thin film. The wafers were freeze-dried in a vacuum extractor for several days. Then the silica wafers were observed on a JEOL JSM-6700F FE-SEM at 3.0 kV.

Fluorescence Microscopy (FM) Observations. A small amount of gel sample was homogeneously dispersed on a cover glass to generate a thin film on the cover glass. The cover glass was freeze-dried in a vacuum extractor for several days and then observed using an inverted microscope (model IX81, Olympus, Tokyo, Japan) equipped with a high-numerical-aperture 60× oil-immersed objective lens (PlanApo, Olympus, Tokyo, Japan), a UV-mercury lamp (OSRAM, HBO, 103w/2, Germany), a mirror unit consisting of a 330−385 nm excitation filter, a 390−460 nm emission filter, and a 16 bit thermoelectrically cooled EMCCD (Cascade512B, Tucson, AZ, USA). The EMCCD was used for collecting the fluorescent images. Imaging acquisition and data analysis were performed using the MetaMorph software (Universal Imaging, Downingtown, PA, USA).

Atomic Force Microscopy (AFM). A drop of solution was placed onto a silica wafer to generate thin films on the wafer. The wafers were frozen in a vacuum extractor at −55 °C for 7 days and then observed using a digital instrument (NanoScope III) that operated in tapping mode. A NSC35/AlBS silicon tip with the cantilever length of 90 μm was employed with the resonance frequency region of 240−405 kHz and a scan rate of 1.0 Hz.

Rheological Measurements. Rheological measurements were performed on a HAAKE RS6000 rheometer with a cone−plate system (C35/1° Ti L07116 at 25.0 ± 0.1 °C, diameter, 35 mm; cone angle, 1°). The viscoelastic properties of the hydrogels were determined by using oscillatory measurements with an amplitude sweep in the frequency range of 0.01 to 10 Hz. Prior to the frequency sweep, the linear viscoelasric region was determined by stress-sweep measurements and the yield stress data.

Differential Scanning Calorimetry (DSC) Measurements. Phase transition temperatures were obtained from DSC8500 (PerkinElmer, Waltham, MA, USA). The heating rate was set as 2 °C·min^{-1}.

Fluorescence Spectroscopy. The fluorescence measurements were performed on a LS-55 spectrofluorometer (PerkinElmer, Waltham, MA, USA) with a quartz cell (1 × 1 cm).

Formaldehyde (HCHO) Removal. 50 mL hydrogels of 50 mmol·L^{-1} PPCT/500 mmol·L^{-1} KOH were added into 100 mL HCHO solution. The variation of HCHO concentration was monitored by UV−vis spectra on HITACHIU-4100 spectrophotometer. The scan rate for each measurement was 120 nm·min^{-1}. The determination of HCHO was used acetylacetone spectrophotometric method (ASM). The principle of this method was that in the existence of excess ammonium salts, HCHO can produce a yellow compound with acetylacetone, which has maximum absorption at about 415 nm. The reaction is shown in eq 1:

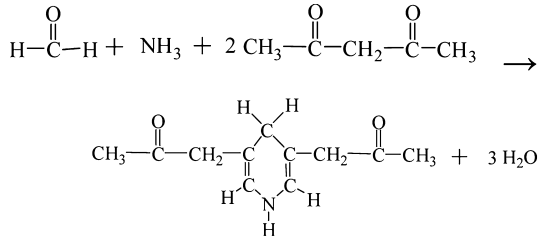

(1)

3. RESULTS AND DISCUSSION

Gelation Behavior. Terpyridine (TP), an excellent ligand, can easily form complexes with metal ions in aqueous solutions and can be used as a metal-gelator.[13] According to the literature,[11,12] the derivative of TP, PPCT was synthesized, and the chemical molecular formula is shown in Figure 1a. PPCT

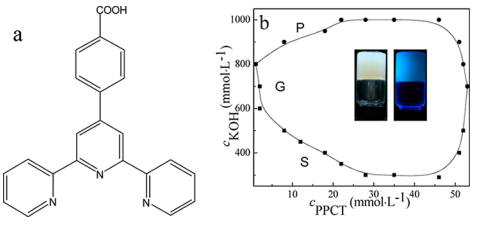

Figure 1. (a) Chemical molecular formula of PPCT, and (b) phase diagram of PPCT/KOH system at 25.0 ± 0.1 °C. The inset sample photos are hydrogels formed by 1 mmol·L^{-1} PPCT mixed with 800 mmol·L^{-1} KOH without the hand-held UV lamp (left) and with the hand-held UV lamp (right).

was characterized by mass spectrometry (MS) and ^{1}H NMR spectroscopy, indicating a higher purity (Figure S1, Supporting Information). Stulz et al.[11] reported that PPCT exhibited specific interaction with Na^+ compared to other cations (particularly Li^+ and K^+) and formed hydrogels only with NaOH at room temperature (R.T.), which prohibits its pratical applications. In our present study, the gelation behaviors of PPCT with different alkalis, MOH (M^+ = Li^+, Na^+, K^+, Cs^+, NH_4^+, $(CH_3)_4N^+$, $(CH_3CH_2)_4N^+$, $(CH_3CH_2CH_2)_4N^+$, $(CH_3CH_2CH_2CH_2)_4N^+$) were detected to examine the effect of monovelent cations on the gelation behaviors, which were seldom reported.[14] Due to the different hydration radius (R_h) of these M^+, the gelation behaviors of PPCT/MOH systems were completely different. The remarkable differences of gelation behaviors, as listed in Table 1, demonstrate the

Table 1. Gelation Property of PPCT/MOH Systems in Aqueous Solutions

	hydration radius, R_h, of M^+/Å[26]	aggregates	CGC (wt %)	gelation time	gelation number
LiOH	3.82	P[a]			
NaOH	3.58	G[b]	0.106	30 min 25 °C	18500
KOH	3.31	G	0.035	10 min 25 °C	55000
NH_4OH	3.31	WG[c]	1.412	5 days 25 °C	1400
Me_4NOH	3.47	WG	1.059	4 months 4 °C	1800
Et_4NOH	4.00	S[d]			
Pr_4NOH	4.52	S			
Bu_4NOH	4.94	S			
CsOH	3.29	WG	0.706	3 months 4 °C	2800

[a]P: precipitates. [b]G: gels. [c]WG: weak gels. [d]S: solutions.

significant role of R_h of M^+ in the gelation process. The gelation capability can be expressed by "critical gelation concentration (CGC)" and "gelation number".[15] The gelation number represents the maximum number of solvent molecules immobilized by per gelator molecule.[16] From Table 1, one can see that PPCT and MOH can form gels only the values of R_h in the range of 3.29 to 3.58 Å. Because the R_h of K^+ is 3.31 Å, thus, KOH has the highest gelation capability with PPCT, the largest gelation number of about 55000 and the fastest gelation time of 10 min. The gelation capability of PPCT/MOH decreases with the increase of R_h of M^+, e.g., Me_4N^+ and Li^+ have lower gelation capability with PPCT. The formation time of hydrogels also increases with the increase of R_h of M^+. When the R_h of M^+ is higher than 3.58 Å, hydrogels can not form in PPCT/MOH systems, only transparent solution or precipitates are obtained. Combined with the law of matching water affinities,[17−19] put forward by Collins, we can concluded that the cations, M^+, should be in a suitable R_h to form hydrogels with the gelator molecules. The reason may be that the R_h of M^+ can greatly affect the electrostatic interaction of M^+ and gelator.[20] The increase of R_h leads to the decrease of charge density, causing the reduce of the electrostatic interaction between M^+ and gelator.[21−24] The R_h of K^+ is suitable for the cavity of PPCT molecule and provides appropriately electrostatic interaction to sustain the balance of the noncovalent interaction between PPCT molecules and K^+ in gelation, inducing the highest gelation capability (Scheme S1, Supporting Information). More information on the gelation formation mechanism is revealed by small-angle X-ray diffraction (SXRD) patterns, as shown in Figure S2 (Supporting Information). The capability of monovalent M^+ inducing PPCT to form hydrogels is $K^+ > Na^+ > Li^+$, which is followed by the Hofmeister series;[25] this is the first observation in gelation behavior for the Hofmeister series. Meanwhile, we observe that all the hydrogels can keep their original properties for more than 1 year since they are prepared, which provides practical applications in materials sciences.

Figure 1b shows the phase behavior of PPCT/KOH system, which is certified by inverted tube observations. The phase boundary is mainly confirmed by the visual observations. Hydrogels can form at lower than 0.1 wt % PPCT; a typical sample image is shown in Figure 1b, which is the equivalent of the composition of 1 mmol·L^{-1} PPCT mixed with 800 mmol·L^{-1} KOH aqueous solutuion. For further detailed study, two series of samples are selected. One is at a fixed KOH concentration with different amounts of PPCT, whereas another is different amounts of KOH with same PPCT concentration. The photos of the samples at a fixed KOH concentration with different amounts of PPCT are shown in Figure S3 (Supporting Information). At a lower PPCT concentration (10 mmol·L^{-1}), the sample is slightly transparent. With the increases in PPCT concentration, the sample becomes opaque, which is attributed to the microstructure transition of the gel.

Microstructure of Hydrogels. FE-SEM and TEM observations were employed to determine the microstructure in PPCT/KOH hydrogels. For FE-SEM and TEM observations, a small amount of sample (without staining) was mounted onto the silicon wafer and copper grid, respectively, and then freeze-dried for several days. Figure 2 shows the images of the hydrogels at c_{KOH} = 500 mmol·L^{-1} with different amounts of PPCT. From the images, the self-assembled structure transition of the hydrogels from "nanoflowers" (NFs), to "dendrimers-like" structure (DDLs), then to "bamboo leaves-like" structure (BLLs), and finally to fibers is clearly observed with the increase of gelators concentration. Three-dimensional (3D) network structures can immobilize water molecules through solvation and surface tension, which is the essential factor in the formation of hydrogels. In Figure 2a,b, the NFs, which consist of fibrils with the diameters of about 100 nm, can be observed clearly when a small amount of PPCT was added to 500 mmol·L^{-1} KOH solution. The TEM images display hierarchically internal structures in NFs.[27] When c_{PPCT} reaches 20 mmol·L^{-1}, the NFs consist of fibrils with a diameter of 200 nm and coexist with a few "leaves-like" structure (LLs), which can be found in the images of the sample, as shown in Figure 2c,d. With the continuous increase of PPCT concentration, NFs disappear and DDLs form, as shown in Figure 2e,f. The DDLs are 3D network fibers with a diameter of 35 nm, a few short fibrils of about 100 nm in width and 1.1 μm in length. When c_{PPCT} is 40 mmol·L^{-1}, BLLs are mainly composed of short fibers with a width of 300 nm and the length of 2 μm (Figure 2g). Cross-linking network fibers with the diameter of 50 nm is observed in Figure 2h,I at c_{PPCT} > 50 mmol·L^{-1}. With careful observations of Figure 2h, one can find a few bundles of fibrils with much larger diameters due to the increase in fibril density, leading to the opacity of the hydrogels at high concentrations. Because the networks formed by the fibril bundles become more and more dense, the structures are hardly observed eventually; we did not give the

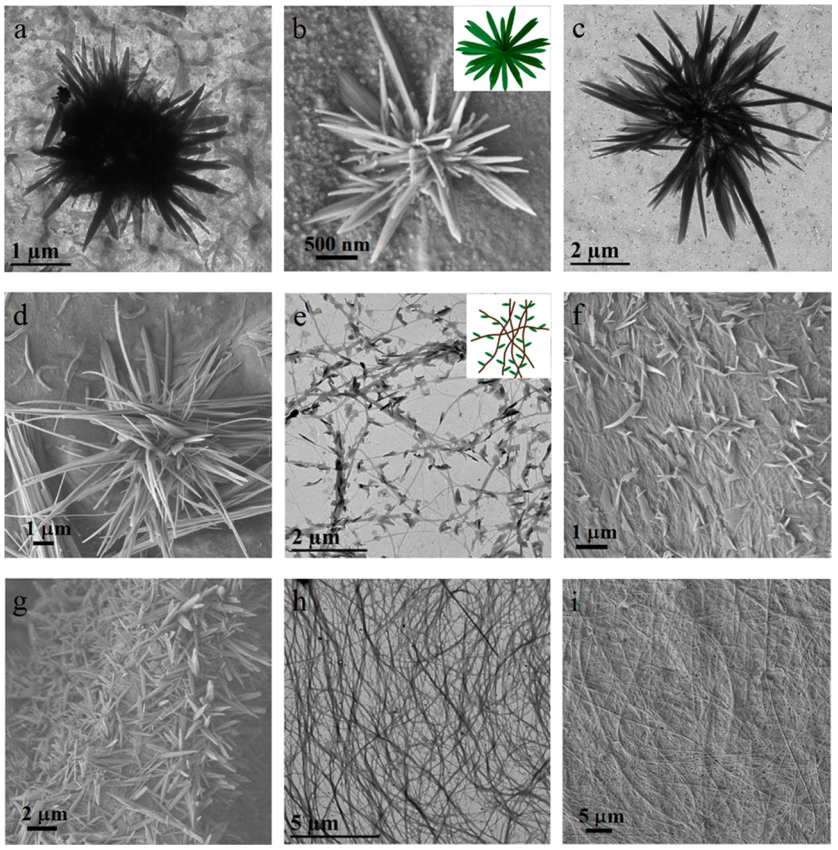

Figure 2. (a, c, e, and h) TEM and (b, d, f, g, and i) SEM images of freeze-dried hydrogels formed by 500 mmol·L^{-1} KOH with different c_{PPCT} (mmol·L^{-1}), (a and b) 10, (c and d) 20, (e and f) 30, (g) 40, and (h and i) 50. The inset pictures are the structure models of the corresponding microstructures of the hydrogels.

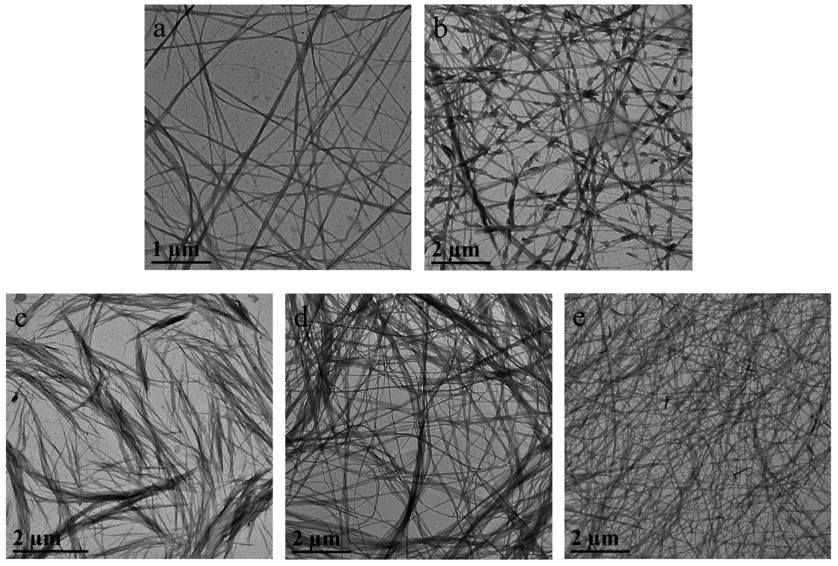

Figure 3. TEM images of freeze-dried gels formed by 30 mmol·L^{-1} PPCT with different c_{KOH}: (a) 400, (b) 600, (c) 700, (d) 800, and (e) 900 mmol·L^{-1}.

electron images of the hydrogel at much higher gelator concentrations.

The morphology change of another series of samples with same amount of PPCT but with the increase of c_{KOH} was characterized by TEM, and the images are shown in Figure 3. The hydrogel sample of 30 mmol·L^{-1} PPCT/400 mmol·L^{-1} KOH consists of fibers with a diameter of 40 nm (Figure 3a). DDLs can be found when c_{KOH} is in the range of 500 to 600 mmol·L^{-1} (Figures 2e,f and 3b). When the KOH concentration reaches 700 mmol·L^{-1}, DDLs disappear and larger BLLs are obtained. When c_{KOH} is above 800 mmol·L^{-1}, long fibers are observed (Figure 3d,e). The width of these fibers ranges from 30 to 50 nm, and their length can be extended to tens of micrometers. These long fibers entangle with each other to

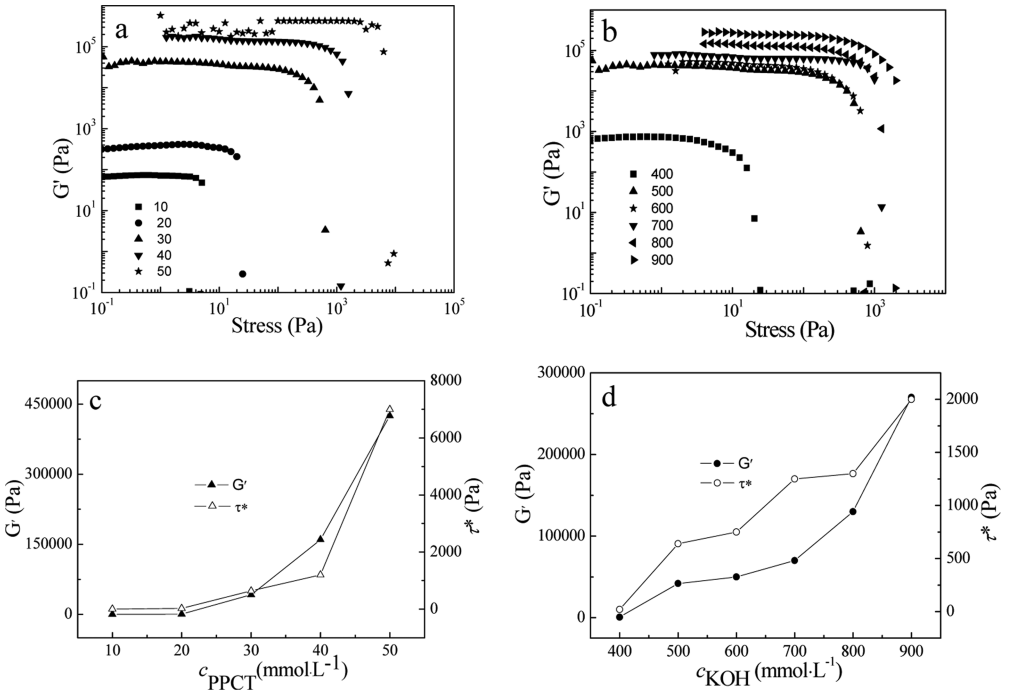

Figure 4. (a) G' as a function of oscillatory stress at c_{KOH} = 500 mmol·L^{-1} with different amounts of PPCT and (b) at c_{PPCT} = 30 mmol·L^{-1} with different amounts of KOH. (c) G' and τ^* as the function of PPCT concentration at c_{KOH} = 500 mmol·L^{-1} and (d) as the function of KOH concentration at c_{PPCT} = 30 mmol·L^{-1}.

form cross-linking networks, which should be the typical feature of hydrogels. The dense degree of the fibers increases with the continuous increase of KOH concentration, resulting in the opacity of the hydrogels at much higher c_{KOH}.

Rheological Property of Hydrogels. The rheological property, an important factor for the applications of gels, is evaluated by measuring the viscoelasticity and the mechanical strength of the gels. The solid-like network structure of the gels that are implanted to be sheared under an increasing stress will break suddenly at a critical shear stress, τ^*, beyond which a Newtonian-like flow occurrs.[9] The τ^* is the so-called "yield stress", reflecting the strength of the microstructure of the gels. We used the oscillatory mode to detect the yield stress of hydrogels at a constant frequency of 1.0 Hz. The influence of PPCT and KOH concentration on the mechanical strength was studied (Figure 4). Figure 4a,c presents that at a fixed KOH concentration of 500 mmol·L^{-1}, the yield stress increases gradually ranging from 5 to 7000 Pa with the increase of PPCT concentration, which could be ascribed to the microstructure transition from NFs to more rigid networks formed by dense fibers. When PPCT concentration reaches 50 mmol·L^{-1}, the yield stress can reach 7000 Pa; comparing the strength of other reported low-molecular-weight hydrogels, our hydrogels present the characteristic of soft viscoelastic solids,[28−30] demonstrating that the networks of the physical entanglement of long fibers have the most rigid property, i.e., the samples have the highest strength. The mechanical strength variation of the hydrogels with the increase of KOH concentration when the PPCT concentration is fixed at 30 mmol·L^{-1} is shown in Figure 4b,d. The self-assembled structure transformation from fibers to DDLs, then to BLLs, and finally to networks induces the increase of yield stress ranging from 20 to 2000 Pa, exhibiting the physical enhancement in mechanical strength. The plateau value of the storage modus, G', in the stress sweep can also be used to evaluate the mechanical strength of hydrogels. One can find that the G' value of the sample also rises with the increase of PPCT or KOH concentration increase, revealing the improvement in mechanical strength (Figure 4c,d).

Gels are viscoelastic soft solid-like materials that simultaneously store and dissipate energy.[29,31] To examine the elasticity and viscosity of gels can not only provide a parameters of materials to guide the application but also supply different models to speculate the microstructure of materials.[32] The viscoelasticity of gels can be characterized by two dynamic moduli: the storage modulus (G'), estimating the degree of resistance against mechanical disturbance, and the loss modulus (G''), measuring the tendency of a material to flow under stress. We performed dynamic rheology to investigate the viscoelastic behavior of PPCT/KOH hydrogels with the concentration variation. Figure S4 (sample frequency sweep, Supporting Information) presents that the sample exhibits higher value of G' than G'' in the whole frequency range, which is typically observed for soft solid-like materials such as gels.[33] Expectedly, the absolute value of G' increases with the increase of PPCT and KOH concentrations. The stiffness/rigidity values of the hydrogels, i.e., the ratio of the dynamic moduli, G'/G'', are found to be 4 to 15, as listed in Tables S1 and S2 (Supporting Information), which further proves that with the increase of PPCT or KOH concentration the fibers arrange more tightly, producing much higher mechanical strength.

Stimuli-Response Properties of Hydrogels. Stimuli-responsive hydrogels supply promising opportunities to design and fabricate new functional materials such as senors, actuators, shape memories, drug delivery devices, etc.[34] For PPCT/KOH hydrogels, the thermoresponsive and mechanical responsive hydrogels were tested (Figure 5). The hydrogels can transform to solution (sol) upon heating, whereas the solution can convert back to the hydrogels upon cooling to R.T. for 30 min. This cycle can be repeated many times. Meanwhile, the

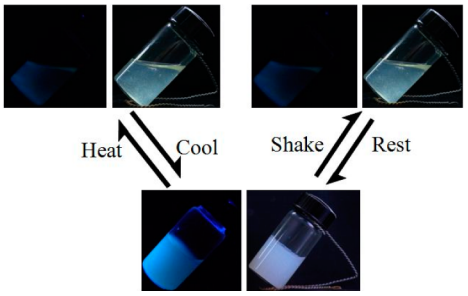

Figure 5. Reversible stimuli-responsive transition of hydrogels with 500 mmol·L^{-1} KOH and 30 mmol·L^{-1} PPCT triggered by shearing forces and temperature. The fluorescence photographs are obtained under a hand-held UV lamp.

hydrogels can be destroyed by shaking the sample vigorously to form a solution, which can recover to hydrogels after being left set for 10 min, which is essential for all biological systems down to the level of tissues and cells.[34]

Hydrogels usually undergo a gel−sol phase transition when the temperature rises, accompanying a reduction of the mechanical strength. The differential scanning calorimetry (DSC) experiments were performed to scrutinize the gel−sol transition temperature ($T_{gel-sol}$) of PPCT/KOH hydrogels. An endothermic peak can be found in the heating curve, indicating a positive transfer enthalpy of gel to sol. The variation of $T_{gel-sol}$ with the increase of PPCT and KOH concentrations is shown in Figure 6. One can find that with the increase of PPCT or KOH concentrations, the endothermic peak shifts to a higher temperature, which is consistent with the variation of mechanical strength of hydrogels. With the increase of PPCT concentration, the self-assembled structure from NFs to cross-linking fibers enhance the mechanical strength of the hydrogels, which requires more energy to destroy the hydrogel and induces the $T_{gel-sol}$ to be a higher value. The increasing of c_{KOH} makes the networks formed by fibrils to be much denser, requesting a higher temperature to break the networks and leading to the increasing in $T_{gel-sol}$. An exothermic peak can also be found in the cooling curve, showing a negative transfer enthalpy of sol−gel. Figure 6a shows that the hydrogels of same concentration melt at 46.83 °C (endothermic peak) and reform at 40.59 °C (exothermic peak). The temperature difference between the exotherm and the endotherm is 6.24 °C, exhibiting the hysterisis.[35]

The microstructure transition of hydrogels induced by temperature and shearing force is shown in Figure 7. As shown in Figure 7a, when the hydrogels are shaken, the DDLs are broken to form small fibrils with a width of 80 nm and length of 500 nm. A probable reason may be that the introduction of energy breaks the balance of the multiple noncovalent interactions in hydrogels, leading to the rearrangement of the PPCT and K^+ cations to destroy the DDLs. When the shaking sample is left resting for 10 min, small fibrils would transform to DDLs again due to the recovery of the balance of the multiple noncovalent interactions between PPCT and K^+ (Figure 7d). When the hydrogels are heated, DDLs can be transformed to a globular structure (Figure 7b), owing to the decrease of R_h of K^+ which causes the increase of its charge density, and leading to the enhancement of electrostatic interaction which produce the rearrangement of PPCT and K^+ (Figure 7f). With the detailed observations, we find that globular structures are not sphere but "Chinese-Gold-Ingots" shaped with a diameter of about 60 nm and length of 150 nm, probably the short fibrils (Figure 7c). DDLs can be obtained, when the heated solution is cooled to R.T. for 30 min (Figure 7e).

Fluorescence Property. The role of $\pi-\pi$ interaction of aromatic rings in the gelation can be monitored by fluorescence

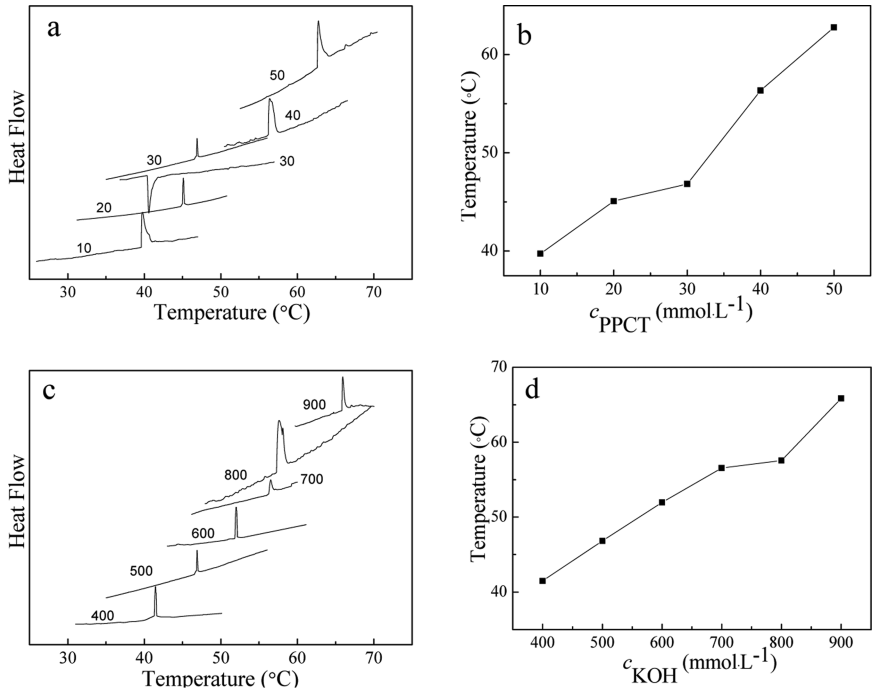

Figure 6. (a) DSC curves of hydrogels of 500 mmol·L^{-1} KOH with different amounts of PPCT and (b) $T_{gel-sol}$ as a function of the concentration of PPCT at c_{KOH} =500 mmol·L^{-1}. (c) DSC curves of hydrogels of 30 mmol·L^{-1} PPCT with different amounts of KOH and (d) $T_{gel-sol}$ as a function of the concentration of KOH at c_{PPCT} =500 mmol·L^{-1}.

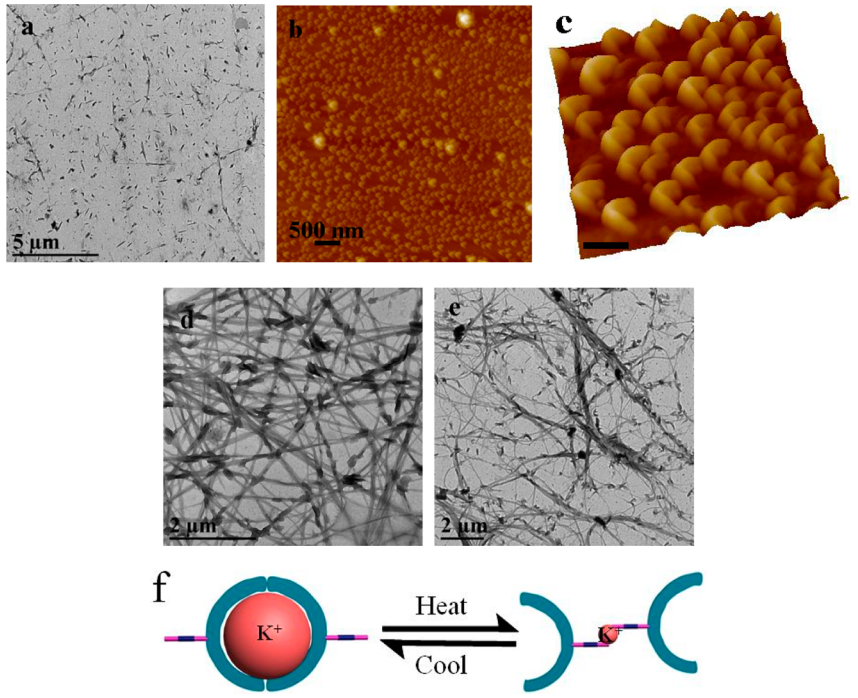

Figure 7. (a, d, and e) TEM images and (b and c) AFM images of hydrogels of 500 mmol·L^{-1} KOH/30 mmol·L^{-1} PPCT: (a) after shaking, (b and c) after heating, (d) at rest for 3 h after shaking, and (e) cooling to room temperature for 3 h. Panel c is the enlarged image of panel b and the bar in panel c is 200 nm. (f) The mechanism model of PPCT/KOH hydrogels in the thermoresponsive process.

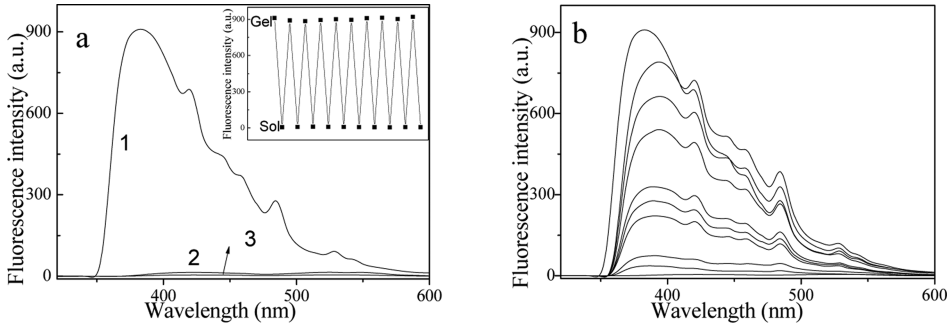

Figure 8. (a) Fluorescence spectra of 30 mmol·L^{-1} PPCT/500 mmol·L^{-1} KOH in hydrogel phase (curve 1), heating the hydrogel to be solution phase (curve 2), and the solution of 30 mmol·L^{-1} PPCT/100 mmol·L^{-1} KOH (curve 3). The inset shows the reversible variation of the emission intensity at 382 nm during the sol−gel phase transition of 30 mmol·L^{-1} PPCT/500 mmol·L^{-1} KOH hydrogel. (b) Change of the fluorescence spectra of the heating solution of 30 mmol·L^{-1} PPCT/500 mmol·L^{-1} KOH hydrogel upon cooling, the time from bottom to top is 0, 2, 5, 10, 12, 15, 20, 22, 25, 30 min. λ_{ex} = 275 nm.[11]

spectra.[36,37] Figure 8a shows PPCT in solution and hydrogel state, respectively, presenting completely different fluorescence spectra (λ_{ex} = 275 nm). In solution (curve 3), the aromatic rings are relatively free and the emission peak at λ_{em} = 382 nm arising from monomeric PPCT molecules is rather weak because of the fluorescence quenching in aqueous solution. While PPCT molecules form hydrogels, the aromatic rings are restricted by the $\pi-\pi$ stacking, leading to the fluorescence enhancement in hydrogel state (curve 1). This kind of fluorescence enhancement after gelation can be referred as gelation-induced enhanced fluorescence emission.[38] When the hydrogels are heated to be solution state, the emission peak intensity at 382 nm is reduced greatly (curve 2), owing to the $\pi-\pi$ stacking elimination in solution state and the fluorescence quenching. When the solution is cooled to be R.T., the fluorescence intensity change with the cooling time is shown in Figure 8b. The fluorescence intensity can be gradually enhanced and recovered to the original intensity when the cooling time reaches to 30 min. Interestingly, such fluorescence variation during the gel−sol phase transition can be reversibly proceeded for time and again (e.g., 10 cycles), as shown in the inset of Figure 8a. This transition can also be observed from the fluorescence photographs in Figure 5. The hydrogel sample has higher fluorescence intensity, while the solution has weak intensity. From the perspective of applications, the hydrogels can be used as a thermal sensors and a thermally driven fluorescence molecular switch.[39] As the hydrogels have much stronger fluorescence intensity, the aggregates formed in the hydrogels could exhibit fluorescence. Confocal laser scanning microscopy (CLSM) can be used to detect the microstructure transition of the hydrogels with the variation of PPCT and KOH concentrations. The self-assembled structure transition of PPCT/KOH hydrogels from NFs to DDLs, then to BLLs, and finally to fibers with the change of PPCT and KOH

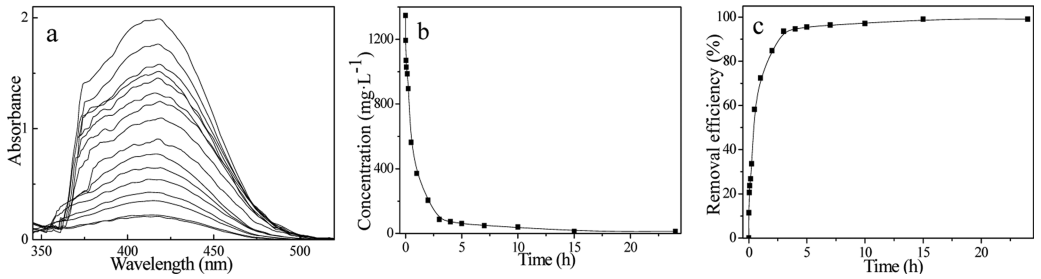

Figure 9. (a) UV−vis spectra of HCHO solution with time after the addition of the hydrogel of 500 mmol·L^{-1} KOH/30 mmol·L^{-1} PPCT. Before the measurements, the solution was diluted. Within 0 to 15 min, the solution was diluted 60 times. At 30 min, 1 and 2 h, the solution was diluted 40, 30, 20 times, respectively. Within 3 to 10 h, the solution was diluted 10 times. The solution at 15 and 24 h was diluted 5 times. The immersion times of the hydrogels in HCHO solution for each UV spectrum from top to bottom were 0, 1, 3, 5, 10, 15, 30 min, 1, 2, 3, 4, 5, 7, 10, 15, and 24 h. (b) HCHO concentration as a function of time, and (c) the HCHO removal efficiency with time.

concentration is clearly shown in Figure S5 (Supporting Information).

Functional Applications of Hydrogels for Removal of Formaldehyde (HCHO). Due to the toxic malodorous nature and the contribution to ozone and smog formation of volatile organic compounds (VOCs), their discharge from chemical industrial plants, vehicles, electroplating, spray-painting, and some organic solvents has been regarded as a serious air pollution problem.[40] Since 2004, HCHO has been considered as one of the dominating VOCs carcinogentic for human.[41] High HCHO concentration has far-reaching impacts on human respiratory, nervous, and immune systems. Long-term exposure to indoor air even containing a few part per million of HCHO may have an adverse influence on human health. Therefore, it is urgent to develop more efficient and convenient approaches for the removal of HCHO. Oxidizing HCHO to carbon oxide through a catalytic process and adsorbing HCHO by an efficient adsorbent are two practical and economic methods to eliminate the HCHO,[42] and a combination of physical adsorption and chemical reaction method is used to eliminate HCHO in this paper, which were seldom reported.[43] The PPCT/KOH hydrogels of 500 mmol·L^{-1} KOH and 50 mmol·L^{-1} PPCT with excellent 3D networks were used to remove HCHO. For the adsorption process, 500 mmol·L^{-1} KOH/50 mmol·L^{-1} PPCT hydrogel (50 mL) was immersed into HCHO aqueous solutions (100 mL) and then left undisturbed.

The acetylacetone spectrophotometric method (ASM) was utilized to determine the HCHO content in solution. The variation of HCHO concentration was monitored by UV−visible spectra after the addition of PPCT/KOH hydrogels. From Figure 9a, it is clearly seen that the HCHO concentration decreases sharply after the addition of PPCT/KOH hydrogels initially, then decreases gradually and reaches an unchanged value after 15 h. Combined with the calibration curve of HCHO solution (Figure S6, Supporting Information), the change of HCHO concentration with the immersion time of the hydrogels is shown in Figure 9b. We can conclude that almost all HCHO can be eliminated within 15 h with a removal amount of 22.5 mg·mL^{-1}, which is much higher than those results reported previously.[42−44] The removal efficiency (R) of HCHO can be calculated as eq 2:

$$R = \frac{C_i - C_e}{C_i} \times 100\% \quad (2)$$

Where C_i and C_e are the initial and equilibrium concentrations, respectively, of the HCHO concentration in solution. The R of HCHO reaches the highest value within 15 min to 1 h. When the immersion time of the hydrogels reaches 4 h, the R is up to 93%. The present method is much more efficient and convenient, which should provide a practical application for indoor HCHO treatment.

According to the literature,[42−44] the HCHO efficient removal mechanism of PPCT/KOH hydrogels is proposed in Figure 10.

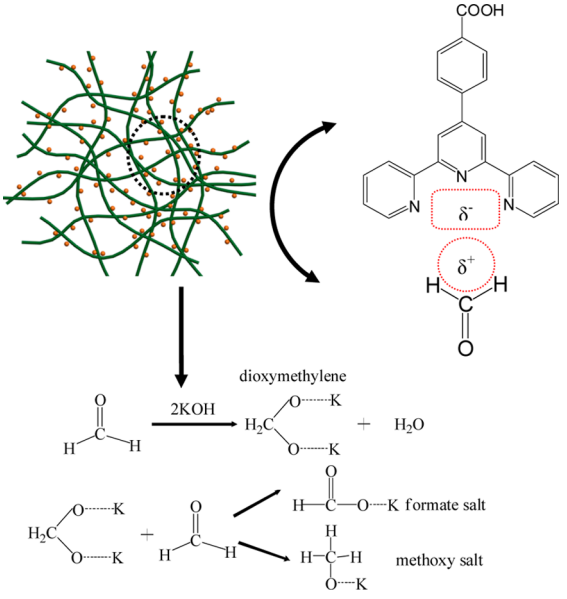

Figure 10. Mechanism of PPCT/KOH hydrogels for the removal of HCHO.

The PPCT molecule has three pyridine rings; the nitrogen atom in the pyridine rings possesses partly negative charge (δ^-), endowing it strong electronegativity, while the carbon atom of HCHO takes slightly positive charge (δ^+), endowing it weaker electronegativity than the oxygen atom. Thus, the HCHO molecule can be efficiently adsorbed onto the network fibers due to the electrostatic interaction between the nitrogen atoms of PPCT and the carbon atom of the HCHO.[44] KOH entrapped in the hydrogels could trigger a nucleophilic-addition transformation from HCHO to dioxymethylene.[45] The formed dioxymethylene can react with another HCHO molecule, in which K and H species from dioxymethylene transfers to the HCHO molecule, with the formation of formate and methoxy salts detected by gas chromatography−mass spectrometry (GC−MS), as shown in Figure S7 (Supporting Information). Thus, we can conclude that the HCHO removal mainly

consists of two processes: physical adsorption through electrostatic interaction and chemical reaction. Combined with the HCHO removal efficiency (Figure 10), the physical adsorption process could be accomplished within 15 min. HCHO reacts with KOH and transforms into nontoxic salts (HCOOK and CH_3OK), corresponding to the highest removal efficiency within 15 min to 1 h. With the reduction of c_{HCHO}, the reaction rate decreases, leading to the reduction of removal efficiency. However, the removal efficiency is very high, e.g., after immersion for about 4 h the removal efficiency can reach 93%. Moreover, this method is convenient and green, promising the application of PPCT/KOH hydrogels for reduction of HCHO in home furnishings, to reduce indoor environmental pollutants.

4. CONCLUSIONS

In summary, the gelation behavior of the PPCT/MOH (M^+ = Li^+, Na^+, K^+, Cs^+, NH_4^+, $(CH_3)_4N^+$, $(CH_3CH_2)_4N^+$, $(CH_3CH_2CH_2)_4N^+$, $(CH_3CH_2CH_2CH_2)_4N^+$) system clearly indicates that the PPCT and KOH mixtures have excellent gelation capabilities due to the appropriate R_h of K^+, providing suitable electrostatic interaction and sustaining the balance of multiple noncovalent interaction between PPCT molecules and K^+. Only if the R_h of M^+ is in a suitable region of 3.29 to 3.58 Å, e.g., K^+, Na^+, and Cs^+, can hydrogels be formed. The ability of M^+ for inducing PPCT to form hydrogels is $K^+ > Na^+ > Li^+$, following by the Hofmeister series. With the increase of PPCT concentration, the self-assembled structure transition of PPCT/KOH hydrogels from NFs to DDLs, then to BLLs, and finally to fibers was observed, corresponding to the mechanical strength enhancement and the $T_{gel-sol}$ elevating. Because the nitrogen atom in the pyridine rings of PPCT molecules possesses a partly negative charge (δ^-), the HCHO molecule, of which a carbon atom exhibits a slightly positive charge (δ^+), can be readily adsorbed onto PPCT/KOH hydrogels through electrostatic interaction. HCHO can be transformed into HOOK and CH_3OK in the presence of KOH. Due to its higher efficiency and convenience, the PPCT/KOH hydrogels can be envisaged as a candidate for functional applications in the removal of indoor HCHO. We hope our results can prompt further theoretical study on the design of amphiphilic hydrogels and provide useful information regarding environmental protection.

■ ASSOCIATED CONTENT

Supporting Information

Chemical structure characterization data of PPCT, formation mechanism of the hydrogels; small-angle X-ray diffraction (SXRD) patterns; photographs of hydrogel; storage modulus (G') and loss modulus (G'') as a function of frequency; fluorescence microscope images; calibration curve of HCHO solution; gas chromatography−mass spectrometry (GC−MS) spectra of HCHO solution after the addition of PPCT/KOH hydrogels. This material is available free of charge via the Internet at http://pubs.acs.org.

■ AUTHOR INFORMATION

Corresponding Author

*J. Hao. E-mail: jhao@sdu.edu.cn. Tel: +86-531-88366074. Fax: +86-531-88564750.

Notes

The authors declare no competing financial interest.

■ ACKNOWLEDGMENTS

This work is financially supported by the NSFC (Grant Nos. 21273134 and 21420102006) and NSF for Distinguished Young Scholars of Shandong Province (JQ201303).

■ REFERENCES

(1) Whitesides, G.; Grzybowski, B. Self-Assembly at All Scales. *Science* **2002**, *295*, 2418−2421.
(2) Moore, J.; Kraft, M. Synchronized Self-Assembly. *Science* **2008**, *320*, 620−621.
(3) Gröschel, A.; Schacher, F.; Schmalz, H.; Borisov, O.; Zhulina, E.; Walther, A.; Müller, A. Precise Hierarchical Self-Assembly of Multicompartment Micelles. *Nat. Commun.* **2012**, *3*, 1−10.
(4) Song, S.; Wang, H.; Song, A.; Hao, J. Superhydrogels of Nanotubes Capable of Capturing Heavy-Metal Ions. *Chem.—Asian J.* **2014**, *9*, 245−252.
(5) Liao, X.; Chen, G.; Jiang, M. Pseudopolyrotaxanes on Inorganic Nanoplatelets and Their Supramolecular Hydrogels. *Langmuir* **2011**, *27*, 12650−12656.
(6) Wu, Z.; Kurokawa, T.; Sawada, D.; Hu, J.; Furukawa, H.; Gong, J. Anisotropic Hydrogel from Complexation-Driven Reorientation of Semirigid Polyanion at Ca^{2+} Diffusion Flux Front. *Macromolecules* **2011**, *44*, 3535−3541.
(7) Tzokova, N.; Fernyhough, C.; Topham, P.; Sandon, N.; Adams, D.; Butler, M.; Armes, S.; Ryan, A. Soft Hydrogels from Nanotubes of Poly(ethylene oxide)-Tetraphenylalanine Conjugates Prepared by Click Chemistry. *Langmuir* **2009**, *25*, 2479−2485.
(8) Weiss, R. The Past, Present, and Future of Molecular Gels. What Is the Status of the Field, and Where Is It Going? *J. Am. Chem. Soc.* **2014**, *136*, 7519−7530.
(9) Zhao, Z.; Lam, J.; Tang, B. Self-assembly of Organic Luminophores with Gelation-Enhanced Emission Characteristics. *Soft Matter* **2013**, *9*, 4564−4579.
(10) Santhosh, B.; Ajayaghosh, A.; Praveen, V. Functional π-Gelators and Their Applications. *Chem. Rev.* **2014**, *114*, 1973−2129.
(11) Griffith, A.; Bandy, T.; Light, M.; Stulz, E. Fluorescent Hydrogel Formation from Carboxyphenyl-Terpyridine. *Chem. Commun.* **2013**, *49*, 731−733.
(12) Constable, E.; Dunphy, E.; Housecroft, C.; Neuburger, M.; Schaffner, S.; Schapera, F.; Batten, S. Expanded Ligands: Bis-(2,2′:6′,2″-terpyridine carboxylic acid)ruthenium(II) Complexes as Metallosupramolecular Analogues of Dicarboxylic Acids. *Dalton Trans.* **2007**, 4323−4332.
(13) Bekiari, V.; Lianos, P. Photophysical Behavior of Terpyridine-Lanthanide Ion Complexes Incorporated in a Poly(N,N-dimethylacrylamide) Hydrogel. *Langmuir* **2006**, *22*, 8602−8606.
(14) Roy, S.; Javid, N.; Sefcik, J.; Halling, P.; Ulijn, R. Salt-Induced Control of Supramolecular Order in Biocatalytic Hydrogelation. *Langmuir* **2012**, *28*, 16664−16670.
(15) Ghosh, A.; Dey, J. pH-Responsive and Thermoreversible Hydrogels of N-(2-hydroxyalkyl)-L-valine Amphiphiles. *Langmuir* **2009**, *25*, 8466−8472.
(16) Song, S.; Dong, R.; Wang, D.; Song, A.; Hao, J. Temperature Regulated Supramolecular Structures via Modifying the Balance of Multiple Non-covalent Interactions. *Soft Matter* **2013**, *9*, 4209−4218.
(17) Collins, K. Charge Density-Dependent Strength of Hydration and Biological Structure. *Biophys. J.* **1997**, *72*, 65−76.
(18) Collins, K. Ions from the Hofmeister Series and Osmolytes: Effects on Proteins in Solution and in the Crystallization Process. *Methods* **2004**, *34*, 300−311.
(19) Collins, K. Ion Hydration: Implications for Cellular Function, Polyelectrolytes, and Protein Crystallization. *Biophys. Chem.* **2006**, *119*, 271−281.
(20) Yan, N.; Xu, Z.; Diehn, K.; Raghavan, S.; Fang, Y.; Weiss, R. Pyrenyl-Linker-Glucono Gelators, Correlations of Gel Properties with Gelator Structures and Characterization of Solvent Effects. *Langmuir* **2013**, *29*, 793−805.

(21) Long, P.; Hao, J. A Gel State from Densely Packed Multilamellar Vesicles in the Crystalline State. *Soft Matter* **2010**, *6*, 4350−4356.
(22) Roy, S.; Javid, N.; Frederix, P.; Lamprou, D.; Urquhart, A.; Hunt, N.; Halling, P.; Ulijn, R. Dramatic Specific-Ion Effect in Supramolecular Hydrogels. *Chem.—Eur. J.* **2012**, *18*, 11723−11731.
(23) Chen, L.; Pont, G.; Morris, K.; Lotze, G.; Squires, A.; Serpell, L.; Adams, D. Salt-induced Hydrogelation of Functionalised-Dipeptides at High pH. *Chem. Commun.* **2011**, *47*, 12071−12073.
(24) Westh, P.; Kato, H.; Nishikawa, K.; Koga, Y. Toward Understanding the Hofmeister Series. 3. Effects of Sodium Halides on the Molecular Organization of H_2O as Probed by 1-Propanol. *J. Phys. Chem. A* **2006**, *110*, 2072−2078.
(25) Hofmeister, F. On the Theory of the Effects of Salts. *Arch. Exp. Pathol. Pharmakol.* **1888**, *24*, 247−260.
(26) Volkov, A.; Paula, S.; Deamer, D. Two Mechanisms of Permeation of Small Neutral Molecules and Hydrated Ions across Phospholipid Bilayers. *Bioelectrochem. Bioenerg.* **1997**, *42*, 153−160.
(27) Núñez, M.; Farley, A.; Dixon, D. Bifunctional Iminophosphorane Organocatalysts for Enantioselective Synthesis: Application to the Ketimine Nitro-Mannich Reaction. *J. Am. Chem. Soc.* **2013**, *135*, 16438−16445.
(28) Cordier, P.; Tournilhac, F.; Soulié-Ziakovic, C.; Leibler, L. Self-Healing and Thermoreversible Rubber from Supramolecular Assembly. *Nature* **2008**, *451*, 977−980.
(29) Hisamatsu, Y.; Banerjee, S.; Avinash, M.; Govindaraju, T.; Schmuck, C. A Supramolecular Gel from a Quadruple Zwitterion that Responds to Both Acid and Base. *Angew. Chem., Int. Ed.* **2013**, *52*, 12550−12554.
(30) Terech, P.; Dourdain, S.; Maitra, U.; Bhat, S. Structure and Rheology of Cationic Molecular Hydrogels of Quinuclidine Grafted Bile Salts. Influence of the Ionic Strength and Counter-ion Type. *J. Phys. Chem. B* **2009**, *113*, 4619−4630.
(31) Pal, A.; Basit, H.; Sen, S.; Aswal, V.; Bhattacharya, S. Structure and Properties of Two Component Hydrogels Comprising Lithocholic Acid and Organic Amines. *J. Mater. Chem.* **2009**, *19*, 4325−4334.
(32) Appel, E.; Loh, X.; Jones, S.; Biedermann, F.; Dreiss, C.; Scherman, O. Ultrahigh-Water-Content Supramolecular Hydrogels Exhibiting Multistimuli Responsiveness. *J. Am. Chem. Soc.* **2012**, *134*, 11767−11773.
(33) Dong, S.; Zheng, B.; Xu, D.; Yan, X.; Zhang, M.; Huang, F. A Crown Ether Appended Super Gelator with Multiple Stimulus Responsiveness. *Adv. Mater.* **2012**, *24*, 3191−3195.
(34) Wang, Q.; Mynar, J.; Yoshida, M.; Lee, E.; Lee, M.; Okuro, K.; Kinbara, K.; Aida, T. High-Water-Content Mouldable Hydrogels by Mixing Clay and a Dendritic Molecular Binder. *Nature* **2010**, *463*, 339−343.
(35) Nanda, J.; Biswas, A.; Banerjee, A. Single Amino Acid based Thixotropic Hydrogel Formation and pH-Dependent Morphological Change of Gel Nanofibers. *Soft Matter* **2013**, *9*, 4198−4208.
(36) Duan, P.; Liu, M. Design and Self-Assembly of L-Glutamate-based Aromatic Dendrons as Ambidextrous Gelators of Water and Organic Solvents. *Langmuir* **2009**, *25*, 8706−8713.
(37) Adhikari, B.; Banerjee, A. Short Peptide based Hydrogels: Incorporation of Graphene into the Hydrogel. *Soft Matter* **2011**, *7*, 9259−9266.
(38) Hong, Y.; Lamab, J.; Tang, B. Aggregation-Induced Emission. *Chem. Soc. Rev.* **2011**, *40*, 5361−5388.
(39) Wang, C.; Zhang, D.; Xiang, J.; Zhu, D. New Organogels Based on an Anthracene Derivative with One Urea Group and Its Photodimer: Fluorescence Enhancement after Gelation. *Langmuir* **2007**, *23*, 9195−9200.
(40) Li, C.; Shen, Y.; Jia, M.; Sheng, S.; Adebajo, M.; Zhu, H. Catalytic Combustion of Formaldehyde on Gold/Iron-Oxide Catalysts. *Catal. Commun.* **2008**, *9*, 355−361.
(41) Salthammer, T.; Mentese, S.; Marutzky, R. Formaldehyde in the Indoor Environment. *Chem. Rev.* **2010**, *110*, 2536−2572.
(42) Nie, L.; Yu, J.; Li, X.; Cheng, B.; Liu, G.; Jaroniec, M. Enhanced Performance of NaOH-Modified Pt/TiO_2 toward Room Temperature Selective Oxidation of Formaldehyde. *Environ. Sci. Technol.* **2013**, *47*, 2777−2783.
(43) Yu, J.; Li, X.; Xu, Z.; Xiao, W. NaOH-Modified Ceramic Honeycomb with Enhanced Formaldehyde Adsorption and Removal Performance. *Environ. Sci. Technol.* **2013**, *47*, 9928−9933.
(44) Song, Y.; Qiao, W.; Yoon, S.; Mochida, I.; Guo, Q.; Liu, L. Removal of Formaldehyde at Low Concentration Using Various Activated Carbon Fibers. *J. Appl. Polym. Sci.* **2007**, *106*, 2151−2157.
(45) Busca, G.; Lamotte, J.; Lavalley, J.; Lorenzelli, V. FT-IR Study of the Adsorption and Transformation of Formaldehyde on Oxide Surfaces. *J. Am. Chem. Soc.* **1987**, *109*, 5197−9202.